Atmospheric
Chemistry
and Physics

Assessing vehicle fuel efficiency using a dense network of CO_2 observations

Helen L. Fitzmaurice[1], Alexander J. Turner[2], Jinsol Kim[1], Katherine Chan[3], Erin R. Delaria[4],
Catherine Newman[4], Paul Wooldridge[4], and Ronald C. Cohen[1,4]

[1]Department of Earth and Planetary Science, University of California Berkeley,
Berkeley, CA 94720, USA
[2]Department of Atmospheric Sciences, University of Washington, Seattle, WA 98195, USA
[3]Program Coordination Division, Sacramento Metro Air Quality Management District,
Sacramento, CA 95814, USA
[4]Department of Chemistry, University of California Berkeley, Berkeley, CA 94720, USA

Correspondence: Ronald C. Cohen (rccohen@berkeley.edu)

Abstract. Transportation represents the largest sector of anthropogenic CO_2 emissions in urban areas in the United States. Timely reductions in urban transportation emissions are critical to reaching climate goals set by international treaties, national policies, and local governments. Transportation emissions also remain one of the largest contributors to both poor air quality (AQ) and to inequities in AQ exposure. As municipal and regional governments create policy targeted at reducing transportation emissions, the ability to evaluate the efficacy of such emission reduction strategies at the spatial and temporal scales of neighborhoods is increasingly important; however, the current state of the art in emissions monitoring does not provide the temporal, sectoral, or spatial resolution necessary to track changes in emissions and provide feedback on the efficacy of such policies at the abovementioned scale. The BErkeley Air Quality and CO_2 Network (BEACO$_2$N) has previously been shown to provide constraints on emissions from the vehicle sector in aggregate over a $\sim 1300\,\mathrm{km}^2$ multicity spatial domain. Here, we focus on a 5 km, high-volume, stretch of highway in the San Francisco Bay Area. We show that inversion of the BEACO$_2$N measurements can be used to understand two factors that affect fuel efficiency: vehicle speed and fleet composition. The CO_2 emission rate of the average vehicle (in grams per vehicle kilometer) is shown to vary by as much as 27 % at different times of a typical weekday because of changes in these two factors. The BEACO$_2$N-derived emission estimates are consistent to within ~ 3 % of estimates derived from publicly available measures of vehicle type, number, and speed, providing direct observational support for the accuracy of the EMission FACtor model (EMFAC) of vehicle fuel efficiency.

1   Introduction

Urban emissions currently account for ~ 75 % of all anthropogenic CO_2 emissions (Seto et al., 2014). By 2050, roughly two-thirds of the Earth's projected population of 9.3 billion is expected to reside within urban areas (Seto et al., 2014), meaning that effective greenhouse gas (GHG) emission reduction strategies must focus on urban emission reductions.

The transportation sector is responsible for ~ 23 % of global GHG emissions worldwide (Seto et al., 2014) and represents the greatest sectoral percentage (~ 25 %–66 %) of emissions from within the boundaries of urban areas in the United States (City of Oakland, 2020; Gurney et al., 2021). Although the fuel efficiency of new internal combustion engine vehicles has increased by ~ 30 % over the last 20 years, and electric vehicles (EVs) are becoming more prevalent (e.g., https://arb.ca.gov/emfac/emissions-inventory, last access: 12 January 2022), emission reductions resulting from fuel efficiency gains in newer vehicles are negated by an in-

creasing percentage of heavy-duty vehicles (HDVs) (Moua, 2020), speed-related reductions in fuel efficiency resulting from increases in congestion, and an increase in the total vehicle kilometers traveled. Over the past 20 years, even in locations with aggressive climate change policies, these factors have resulted in CO_2 emissions from vehicles that have increased or stayed nearly constant. For example, the California Air Resources Board estimates that per capita vehicle emissions in the state of California in 2015 were only 2 % lower than in 2000, and per capita vehicle kilometers traveled increased ~ 2.5 % over that time period (California Air Resources Board, 2018). In addition to GHG emissions, the transportation sector is responsible for a significant share of fine particulate matter ($PM_{2.5}$) and NO_x emissions, exacerbating $PM_{2.5}$ and ozone exposure in BIPOC already experiencing disproportionate health burdens associated with poor air quality (Tessum et al., 2021).

Municipal and regional governments have increasingly shown interest in tracking and reducing CO_2 emissions from all sectors, including transportation. For example, Boswell et al. (2019) found that 64 % of Californians live in a city with a climate action plan. For urban and regional governments to plan, monitor, and responsively adjust emission reduction policies, an up-to-date understanding of the spatial and temporal variations in total emissions and in emissions by sector and subsector processes is key.

For transportation, reductions in vehicle kilometers, congestion mitigation, and rules affecting fleet composition (e.g., limiting road access to HDVs, incentivizing use of electric vehicles, or buy-backs of older vehicles) are three levers that can be employed to reduce CO_2 and AQ emissions from vehicles, thereby affecting the climate footprint, air quality (AQ), and environmental justice (EJ) in a region. However, the current state of the art in emission monitoring and modeling do not provide the temporal, sectoral, or spatial resolution necessary to track changes in urban emissions and provide feedback on the efficacy of each lever separately. Furthermore, current estimates of the magnitude and sectoral apportionment of urban CO_2 emissions can vary widely. For example, Gurney et al. (2021) show how a consistent approach to total emissions from cities across the United States differs from locally constructed inventories in magnitude and sector by sector.

Spatial and temporal process-level maps of emissions are needed to improve the scientific basis for emission control strategies. The current state of the art involves finding aggregate emissions over large regions (e.g., counties or states) using economic data and then downscaling those totals using proxies such as road length, building type, or population density. These models meet the need for high spatial resolution (~ 500 m) and capture emissions from many detailed subsectors (Gately et al., 2015; Gurney et al., 2012; McDonald et al., 2014). Because fuel sales are well characterized, these models are also likely to produce accurate region-wide CO_2 emission totals from the transportation sector.

However, even the most detailed of these inventories do not presently describe the temporal variability in processes that affect emissions, such as the direct response of home heating or air conditioning to ambient temperature or, with one exception (Gately et al., 2017), the variations in emissions per kilometer when comparing free-flowing with stop-and-go traffic. These models often disagree with one another spatially (Gately and Hutyra, 2017), have been subject to only limited testing against observations of the atmosphere, and are not designed to be consistent with separately constructed AQ inventories that have been subject to much more extensive testing against observations.

Mobile monitoring campaigns and high-density measurement networks highlight the importance of characterizing and identifying the processes contributing to sharp neighborhood-scale AQ and GHG hot spots and point to the importance of traffic emissions at neighborhood scales. For example, Apte et al. (2017) showed that concentrations of NO_x and black carbon (BC) can vary by as much as a factor of ~ 8 on the scale of tens to hundreds of meters. Caubel et al. (2019) showed BC concentrations to be ~ 2.5 times higher on trucking routes than on neighboring streets. Such gradients are not represented in inventories based on downscaled economic data.

Observations of CO_2 and other GHGs can play an important role in improving and maintaining the accuracy of emission models – especially during a time of rapid proposed changes. CO_2 measurements paired with Bayesian inverse models have been shown to provide a quantitative assessment of emissions (Lauvaux et al., 2016, 2020; Turner et al., 2020a). To date, most attempts at quantifying urban CO_2 emissions have focused on extracting a temporally averaged (often a full year) total of the anthropogenic CO_2 across the full extent of city. A few studies have attempted to disaggregate emissions by sector or fuel type or to describe large shifts in aggregate emissions (Newman et al., 2016; Nathan et al., 2018; Lauvaux et al., 2020; Turner et al., 2020a), but none characterize the subsector processes of vehicle emissions.

High-spatial-density observations offer promise as a means to explore process-level emission details. The BErkeley Air Quality and CO_2 Network (BEACO₂N) is an observing network deployed in the San Francisco Bay Area and other cities with a measurement spacing of ~ 2 km (Fig. 1, left). In a prior analysis, Turner et al. (2020a) showed that BEACO₂N measurements can detect variation in CO_2 emissions with time of the day and day of the week in addition to the dramatic changes in CO_2 emissions due to the COVID-related decrease in driving.

Here, we analyze hourly, spatially allocated CO_2 emissions derived from the inversion of BEACO₂N observations (Turner et al., 2020a) to explore how well they constrain the CO_2 emissions from a 5 km stretch of highway. This stretch was chosen because of its location upwind of consistently active BEACO₂N sites, for completeness of traffic data, and
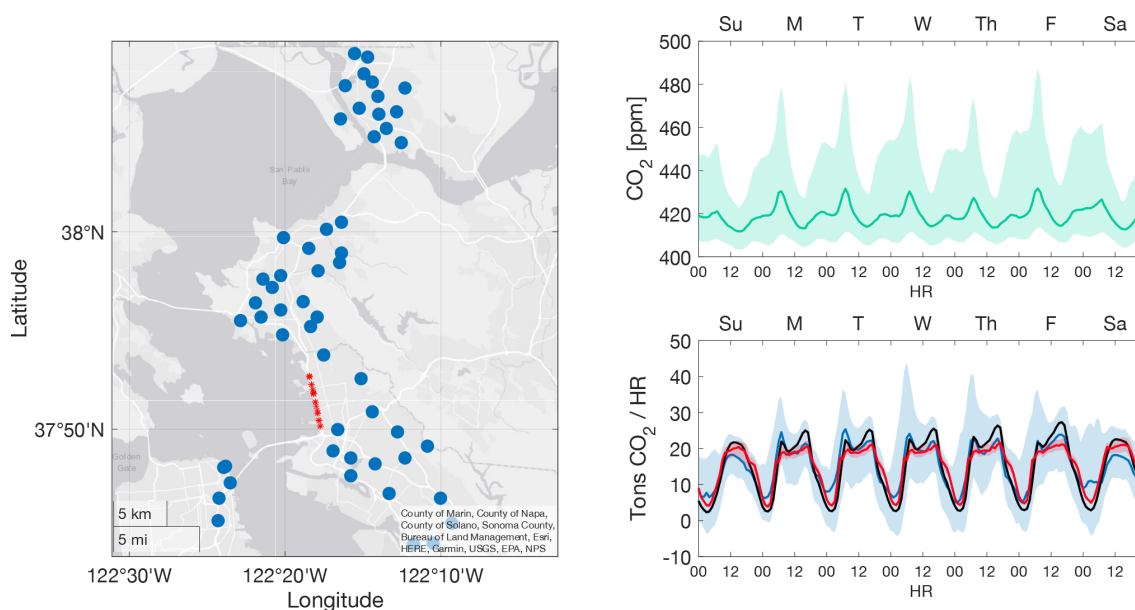
Figure 1. The left panel presents a map of the BEACO$_2$N network, showing all sites (blue dots) for which there are more than 4 weeks of data during the period analyzed (January to June from 2018 to 2020). Red stars indicate the location of the PeMS monitors used in this study. The top right panel presents CO$_2$ values shown for a "typical week" during the time period observed. The dark line represents the median value observed across all sites and times, and the shaded envelope represents 1σ variance across the network and over the 2-year period. The bottom right panel presents CO$_2$ emissions on all highway pixels in the domain as derived from the inversion of BEACO$_2$N observations (blue), BEACO2N prior (black), and the PeMS-EMFAC-based estimate (red). The shaded envelope shows variance in emissions during the 18-month analysis window.

because emission rates are highly affected by speed (vehicles use more fuel per kilometer at very low and high speeds) and fleet composition (HDVs emit more CO$_2$ per kilometer than light-duty vehicles, LDVs). The variation in the ratio of total fleet CO$_2$ emissions per vehicle kilometer traveled (grams of CO$_2$ per vehicle kilometer) is used to explore variations in on-road fuel efficiency and the factors responsible for that variation. We show that the average fuel efficiency of the vehicle fleet on the road varies by as much as 27 % over the course of a typical weekday.

2   Methods and data

2.1   The Berkeley Air quality and CO$_2$ Network

We use hourly CO$_2$ observations from the Berkeley Air quality and CO$_2$ Network (BEACO$_2$N) (Shusterman et al., 2016; Kim et al., 2018; Delaria et al., 2021). The BEACO$_2$N network includes more than 70 locations in the San Francisco Bay Area, spaced at ~ 2 km, and measures CO$_2$ with a network instrument error of 1.6 ppm or less (Delaria et al., 2021). All available data from January to June during the 2018–2020 period are included in this analysis. During this time, more than 50 distinct locations had nodes that were active for a month or more (including 19 sites within 10 km of our highway stretch of interest). The number of nodes active at any given time ranged from 7 to 41, with a mean of

17. Figure 1 shows sites in operation at some point during analysis period, and Fig. S1 in the Supplement shows a time series of the number of nodes available throughout the study period.

2.2   The BEACO$_2$N Stochastic-Time Inverted Lagrangian Transport inversion system (BEACO$_2$N-STILT)

To infer CO$_2$ emissions from within the BEACO$_2$N footprint, we use the Stochastic-Time Inverted Lagrangian Transport (STILT) model, coupled with a Bayesian inversion as described in detail in Turner et al. (2020a). Briefly, we use meteorology from the National Oceanic and Atmospheric Administration (NOAA) High-Resolution Rapid Refresh (HRRR) product at a 3 km resolution to calculate footprints from each hour at each site, weighted by a priori CO$_2$ emissions. The overall region of influence, the network footprint, as defined by a contour representing 40 % of the CO$_2$ influence, is shown in Fig. S2 (left). We construct a spatially gridded prior emission inventory using point sources provided by the Bay Area Air Quality Management District (BAAQMD) (2015), home heating emissions as reported by BAAQMD (2011) and distributed spatially according to population density, on-road emissions from the High-resolution Fuel Inventory for Vehicle Emissions (McDonald et al., 2014) varying by hour of week and scaled by year us-

ing fuel sales data, and a biogenic inventory derived using solar-induced fluorescence (SIF) satellite data (Turner et al., 2020b).

To ensure a focus on highway emissions, we subtract prior estimates associated with non-highway sources from posterior BEACO$_2$N-STILT fluxes. Non-highway sources are small ($\sim 12\%$) in comparison with highway emissions for the pixels corresponding to the highway stretch analyzed in this study (Fig. 2, left). We assume the error in prior estimates of these sources to be an even smaller fraction of the total. For reference, a diel cycle of sector-specific, weekday prior emissions for the pixels analyzed in this study is shown in Fig. S3.

We estimate the BEACO$_2$N-STILT inversion to be precise to at least 30 % for a line source. This estimate is based on the results of Turner et al. (2016), who used observation system simulation experiments to demonstrate that a 45 tC h^{-1} line source could be constrained to 15 tC h^{-1} with 7 d of observations at 30 sites. However, this paper also demonstrated that error in the posterior decreased as results were averaged over a longer period of time. Here, as we are using 18 months (rather than 7 d) of observations, we expect and observe better precision than 30 %.

2.3 PeMS-EMFAC-derived CO$_2$ emission estimates

Total hourly vehicle flow, the HDV (truck) percentage, and speed were retrieved from http://pems.dot.ca.gov (last access: 12 January 2022) for the period from January to June for the years from 2018 to 2020. There are ~ 1800 traffic counting stations hosted by the Caltrans Performance Measurement System (PeMS) in the San Francisco Bay Area, including more than 400 sites (Fig. S2) within the 2020 footprint of the BEACO$_2$N network, as described in Turner et al. (2020a). These stations count vehicle flow using magnetic loops imbedded in roadways and estimate the HDV fraction using calculated vehicle speed and assumptions about vehicle length (Kwon et al., 2003). For hours during which fewer than 50 % of measurements were reported, we fill in the total speed and light-duty vehicle (LDV) flow gaps using linear fits to nearest-neighbor sites, and we fill in gaps in the HDV flow using hour-of-day-specific and weekend/weekday-specific median ratios between neighboring sites. Using this imputation method, we find that mean absolute errors in speed are 5–10 km h^{-1}, mean absolute errors in the LDV flow are 500 vehicles per hour, and mean absolute errors in the HDV flow are 50 vehicles per hour (see Fig. S4).

We calculate both LDV and HDV vehicle kilometers for each highway segment during each hour using downloaded flow data at each sensor location and segment lengths obtained from the PeMS database. For highway segments within the BEACO$_2$N footprint, vehicle kilometers are summed to obtain regional highway HDV and LDV vehicle kilometers for every hour. Figure S2 (left) shows the extent of

the PeMS network in comparison to the BEACO$_2$N-STILT footprint as well as the total HDV vehicle kilometers and the total LDV vehicle kilometers.

Vehicle fuel efficiency is dependent on both fleet composition and vehicle speed. We calculate an emission rate at each location by combining the speed and the HDV percentage with fuel efficiency estimates provided by the California Air Resources Board EMission FACtor model (EM-FAC2017). The EMFAC2017 model provides yearly fuel efficiency estimates for the San Francisco Bay Area for 41 vehicle classes as a function of speed. We group these 41 vehicle types into the LDV or HDV categories (Table S1). The PeMS vehicle-type classification system is length based, assuming that LDVs have a median length of 3.7 m and HDVs have a median length of 18.3 m (Kwon et al., 2003). As a result, we group most light-duty trucks into the LDV category. To find speed-dependent emission rate values for the LDV and HDV groups, we find a vehicle-kilometer-weighted mean of emission rates across all vehicle classes within a group at a given speed:

$$\text{er}_{\text{speed,group}} = \frac{\sum_{i=1}^{n} \text{vkm}_{i,\text{speed}} \text{er}_{i,\text{speed}}}{\sum_{i=1}^{n} \text{vkm}_{i,\text{speed}}}, \quad (1)$$

where er denotes the total emission rate, i is a vehicle class, and vkm denotes vehicle kilometers. From this, we generate LDV and HDV emission rates at 8.02 km h^{-1} (5 mph) intervals (see Fig. S5). EMFAC does not provide data for several LDV vehicle classes at and above 96.8 km h^{-1} (60 mph). To fill this gap, we estimate emission rates for the LDV group by employing the emission rate to speed slopes (grams of CO$_2$ per vehicle kilometer per hour) for high speeds (88–145 km h^{-1}), using data from Davis et al. (2021).

We calculate emission rates (grams of CO$_2$ per vehicle kilometer) for each (< 1 km) road segment between the PeMS sensors at a moment in time:

$$\text{er}(t,\text{seg}) = \frac{\begin{array}{c}\text{vkm}_{\text{LDV}}(t,\text{seg})\text{er}_{\text{LDV}}(t,\text{seg}) + \text{vkm}_{\text{tHDV}}\\(t,\text{seg})\text{er}_{\text{tHDV}}(t,\text{seg})\end{array}}{\text{vkm}_{\text{LDV}}(t,\text{seg}) + \text{vkm}_{\text{HDV}}(t,\text{seg})}, \quad (2)$$

where the emission rates for cars and trucks are found via a spline fit between the reported speed for that segment and time with our curves for the emission rates of each vehicle group. A fit is used rather than individual bins, due to the sharp gradients that exist at low speeds for LDVs. From the emission rate for each (~ 1 km) segment, we calculate an emission rate for a stretch of highway including several segments to find the total emission rate (er) along a "stretch" over a period of time:

$$\text{er}(t,\text{stretch}) = \frac{\sum_{\text{all segments}}(\text{vkm}_{\text{LDV}})(t,s)\text{er}_{\text{LDV}}(t,s)}{\sum_{\text{all segments}}(\text{vkm}_{\text{LDV}}(t,s)}. \quad (3)$$
$$\frac{+\text{vkm}_{\text{HDV}}(t,\text{seg})\text{er}_{\text{HDV}}(t,s)}{+\text{vkm}_{\text{HDV}}(t,s))}$$

The total CO$_2$ emission rates for the highway stretch analyzed in this work are shown in Fig. 2 (bottom right).
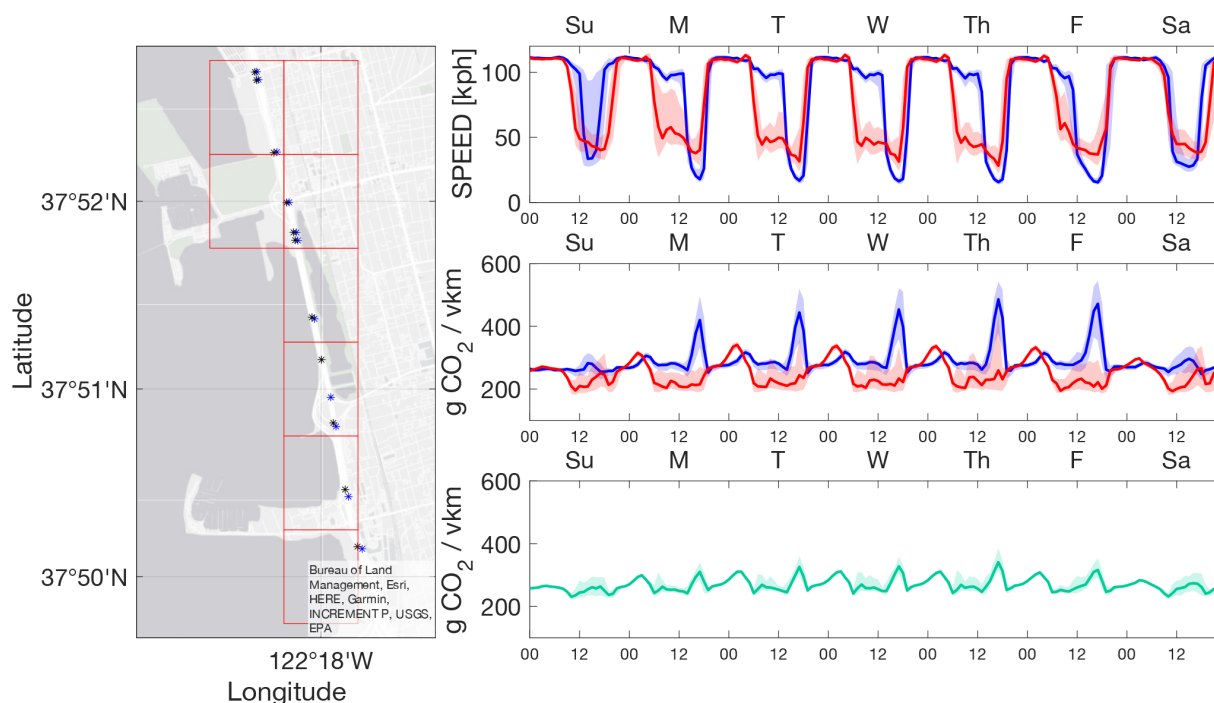
Figure 2. The left panel shows the ~ 5 km stretch over which we analyze grams of CO$_2$ per vehicle kilometer (vkm). Points show the location of PeMS stations, and squares show the pixels associated with BEACO$_2$N-STILT output that we use for comparison for the 5 km stretch. The top right panel presents the hourly average speed shown for two opposite (west in red, and east in blue) PeMS measurement stations for a typical week. The middle right panel presents the PeMS-EMFAC-derived emission rates calculated for two opposite (west in red, and east in blue) PeMS measurement stations for a typical week. The bottom right panel presents the aggregate PeMS-EMFAC-derived estimated emission rates from the two directions of traffic for a typical week for this highway stretch.

3 Results

To gain insight into the relative impacts of congestion and fleet composition, we first calculate fleet-wide vehicle emission rates (in grams of CO$_2$ per vehicle kilometer) using two different methods. For both methods, the Caltrans Performance Measurement System (PeMS; http://pems.dot.ca.gov, last access: 12 January 2022) provides vehicle counts, speed, and vehicle category (HDVs or LDVs). Using these data and estimates of fuel consumption per kilometer from the EMission FACtor 2017 (EMFAC) model, we calculate the CO$_2$ emissions per kilometer for the average vehicle with an hourly time resolution, as described above. Second, we use the PeMS data in combination with the grams of CO$_2$ per unit area derived from the BEACO$_2$N-STILT inversion system. We focus on the ~ 5 km stretch of Interstate 80 just north of the San Francisco–Oakland Bay Bridge (Fig. 2). Interstate 80 is an east–west Highway whose orientation along this stretch is mainly north–south, with eastbound lanes traveling north and westbound lanes traveling south. The road has five lanes in each direction and is often subject to high congestion (vehicles traveling slower than the posted speed).

PeMS-EMFAC-derived emission rates give us insight into (1) the expected variation in emission rates across a typical day (Fig. 2) and (2) the relative impacts of congestion

vs. the HDV percentage as factors leading to this variation (Fig. S6). For example, while the westbound segment experiences speeds significantly below free-flow during both morning and evening rush hours, the eastbound segment experiences significant congestion only during the evening. Because of a steep gradient in LDV emission rates between 20 and 50 km h^{-1} (Fig. S5), the westbound congestion in this segment occurs at speeds that are more fuel efficient than free flow. The overall variance in emission rates over the whole stretch is significantly smaller than in either of the directions shown individually.

From PeMS-EMFAC-derived emission factors, we predict a median diel cycle with the emissions per kilometer traveled ranging from ~ 247 to ~ 314 g CO$_2$ per vehicle kilometer. For reference, if all vehicles were driving at the speed limit of 104.6 km h^{-1} (65 mph) and the fleet mix was 6 % HDVs and 94 % LDVs, we calculate an emission rate of 265 g CO$_2$ per vehicle kilometer. The range of predicted emissions is narrower on the weekend (238–276 g CO$_2$ per vehicle kilometer), as fewer HDVs use the road and there is a smaller range with respect to speed.

Figure S6 shows the hourly variation in the relative contributions of LDV speed, HDV percentage, and HDV speed to the deviation in grams of CO$_2$ per vehicle kilometer from the reference value of 265 g CO$_2$ per vehicle kilometer. The

solid line is the mean, and the shaded envelope represents the day-to-day variance. In the morning and at midday, the HDV percentage and LDV speed have opposite impacts on the grams of CO_2 per vehicle kilometer, leading to small variations in the grams of CO_2 per vehicle kilometer over the day, despite substantial variations in the separate effects of speed and HDV percentage. During evening rush hour, low vehicle speeds result in higher emission rates, leading to large positive deviations. High day-to-day variance in vehicle speed contributes to high day-to-day variance in emission rates. At times near midnight, large, positive deviations are observed, mostly as a consequence of a high HDV percentage but also because traffic flows at rates higher than $104.6\,\mathrm{km}\,\mathrm{h}^{-1}$, leading to higher emission rates. Night-to-night variance in the HDV percentage is low; thus, variance in the nighttime predicted grams of CO_2 per vehicle kilometer is small. The HDV speed has little impact on the grams of CO_2 per vehicle kilometer.

We use CO_2 measurements from 50 BEACO$_2$N sites across the San Francisco Bay Area combined with the BEACO$_2$N-STILT inversion system to assess highway emissions from our stretch of interest. In Fig. 1, we show the location of BEACO$_2$N sites, the stretch of interest, and emission estimates for this stretch. Note that the posterior emissions move substantially from prior emissions towards what is estimated from PeMS-EMFAC, particularly during the evening rush hour, when the prior overestimates emissions by $\sim 20\,\%$.

We compare BEACO$_2$N-derived and PeMS-EMFAC-derived emission rates (grams CO_2 per vehicle kilometer) and find remarkable agreement. The PeMS-EMFAC-derived emission rates range from 225 to $300\,\mathrm{g}\,CO_2$ per vehicle kilometer and include the effects of both fleet composition and variation in speed. For BEACO$_2$N, we use the total CO_2 emissions from the inversion at times corresponding to narrow bins of PeMS-EMFAC (grams of CO_2 per vehicle kilometer). Figure 3a shows an example of data selected at times with PeMS-EMFAC-derived fuel efficiency in the range of 271.4 to $279\,\mathrm{g}\,CO_2$ per vehicle kilometer. There is a range of emissions at each vehicle kilometer because of noise in the inversion, variation in speed, and variation in the fleet composition. The slope of a fit to the data in Fig. 3a is an estimate of the emission rate (Eq. 4), where CO_2 emissions are defined as hourly emissions summed over BEACO$_2$N pixels corresponding to our highway stretch of interest (Fig. 2):

$$\mathrm{er}\left(\mathrm{g}\,CO_2\,\mathrm{vkm}^{-1}\right) = \frac{CO_2\ \mathrm{emissons}}{\mathrm{vkm}}. \tag{4}$$

Using 18 months of data for weekdays between 04:00 and 22:00 local time, we compare PeMS-EMFAC-derived and BEACO$_2$N-derived CO_2 per vehicle kilometer (Fig. 3b). These hours were chosen, because they represent the hours for which we expect traffic emissions to be substantially larger than emissions from other sources in our area of interest (see Fig. S3). When fitting to a line forced through

the origin, emission rates found via the BEACO$_2$N inversion are within $3\,\%$ (0.97 ± 0.01) of those predicted using PeMS-EMFAC traffic counts. A more complete description of this fitting and error calculation process can be found in Sect. S8, and a comparison to the results from applying this method to the prior can be found in Sect. S9. Using the definition of the limit of detection as 3 times our uncertainty, we calculate that we would be able to detect an $11\,\%$ change in individual points (representing bins of fuel efficiency from a combination of HDV percentage and speed) and a $3\,\%$ change in the slope. Because 18 months of data was required to reach this level of certainty, if we assume the $2.3\,\%$–$3.8\,\%\,\mathrm{yr}^{-1}$ decrease in the emission rate found by Kim et al. (2021), we should be able to detect a change in the overall fuel efficiency with 3 full years of BEACO$_2$N-STILT output.

We also consider how emission rates compare throughout the day (Fig. 4a). During the evening, PeMS-EMFAC-derived and BEACO$_2$N-derived emission rates are in good agreement. The BEACO$_2$N grams of CO_2 per vehicle kilometer increases from $256\,\mathrm{g}\,CO_2$ per vehicle kilometer before rush hour (14:00) to $324\,\mathrm{g}\,CO_2$ per vehicle kilometer during peak rush hour (17:00). Likewise, the PeMS-EMFAC-derived CO_2 per vehicle kilometer increases from 256 to $320\,CO_2$ per vehicle kilometer over the same time period. The BEACO$_2$N prior has a slightly larger increase in the emission rate over this period ($256\,\mathrm{g}\,CO_2$ per vehicle kilometer at 14:00 to $361\,\mathrm{g}\,CO_2$ per vehicle kilometer at 17:00). In contrast, during the morning rush hours, we see less agreement between PeMS-EMFAC-derived and BEACO$_2$N-derived emission rate estimates. The BEACO$_2$N inversion is similar to the PeMS-EMFAC estimate at 05:00 local time ($280\,\mathrm{g}\,CO_2$ per vehicle kilometer), and the BEACO2N estimate then increases over the morning rush hour to $330\,\mathrm{g}\,CO_2$ per vehicle kilometer at 8:00. This behavior is different from both the BEACO$_2$N prior ($175\,\mathrm{g}\,CO_2$ per vehicle kilometer at 05:00 and $275\,\mathrm{g}\,CO_2$ per vehicle kilometer at 08:00) and the PeMS-EMFAC calculation which decreases over this period ($275\,\mathrm{g}\,CO_2$ per vehicle kilometer at 05:00 and $250\,\mathrm{g}\,CO_2$ per vehicle kilometer at 08:00).

The discrepancy in the morning between emissions derived from PeMS-EMFAC and BEACO$_2$N can potentially be reconciled by congestion. There is a nonlinear relationship between vehicle speed and the rate of emissions. As such, congestion involving nonconstant speeds can result in higher emissions than would be estimated using the average vehicle speed. This can be seen from a simple example. Consider two cases: (1) an LDV traveling at a constant $50\,\mathrm{km}\,\mathrm{h}^{-1}$ for 1 h and (2) an LDV traveling at $100\,\mathrm{km}\,\mathrm{h}^{-1}$ for 20 min and at $25\,\mathrm{km}\,\mathrm{h}^{-1}$ for 40 min. Both vehicles travel 50 km in 1 h and, therefore, have the same average speed; however, the emission rate is $461.5\,\mathrm{g}\,CO_2$ per vehicle kilometer at $25\,\mathrm{km}\,\mathrm{h}^{-1}$, $195\,\mathrm{g}\,CO_2$ per vehicle kilometer at $50\,\mathrm{km}\,\mathrm{h}^{-1}$, and $221\,\mathrm{g}\,CO_2$ per vehicle kilometer at $100\,\mathrm{km}\,\mathrm{h}^{-1}$. Using these emission rates, the vehicle in the first case would emit 9.75 kg of CO_2,
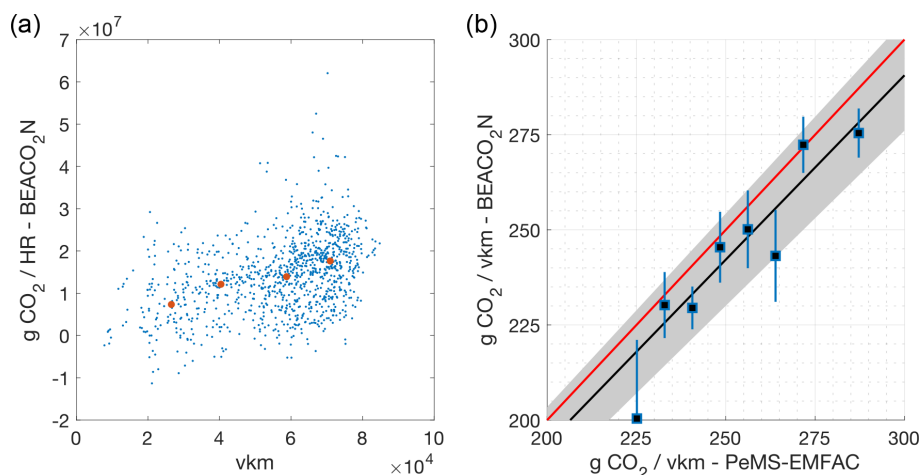
Figure 3. (a) BEACO$_2$N-derived emissions vs. vehicle kilometers (vkm) for times corresponding to modeled emission rates of 271.4–279 g CO$_2$ per vehicle kilometer. Red points represent binned medians used in fitting. **(b)** BEACO$_2$N-derived vs. PeMS-EMFAC-derived emission rates with the uncertainty estimate. The black line shows the fit weighted by variance: $y = 0.97(.01)x$. The gray envelope is the 5 % deviation from fit, and the red line represents the 1 : 1 line.
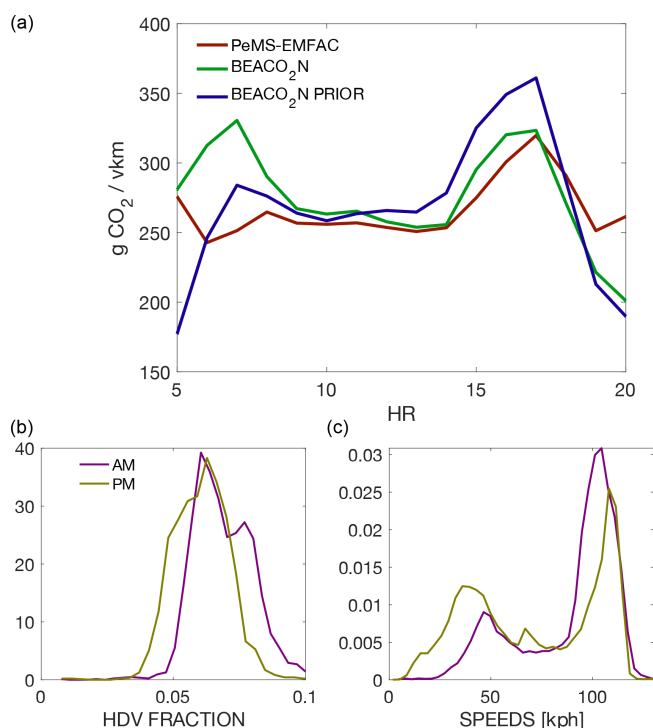
Figure 4. (a) Emission rates by time of day on weekdays for PeMS-derived (red), BEACO2N prior (blue), and BEACO$_2$N posterior (green) data. Probability density functions of the HDV (truck) fraction **(b)** and speed **(c)** from a weekday morning (05:00–09:00) and evening (16:00–20:00) rush hour period on the segment of Interstate 80 analyzed in Sect. 3. The y axis represents the relative probability of the HDV fraction **(b)** or averaged hourly speed **(c)**. Speeds are from individual PeMS sensors, whereas the HDV fraction is aggregated over the whole stretch under consideration (both directions).

whereas the vehicle with the variable speed in the second case would emit 15 kg of CO$_2$.

Contrasting the speeds (Fig. 4c) during these two periods, we see that while both show a bimodal speed distribution, a greater fraction of morning speeds fall into the 40–100 km h^{-1} range, whereas a greater fraction of evening speeds are < 40 or > 100 km h^{-1}. In Fig. S8, we show that emission rate estimates based on hourly averaged speeds between 0 and 40 km h^{-1} and between 100 and 140 km h^{-1} (more common in evening rush hour) are likely an upper bound on possible emission rates corresponding to those hourly averaged speeds, whereas emission rate estimates based on hourly averaged speeds between 40 and 100 km h^{-1} (more common in morning rush hour) likely represent a lower bound of emissions. The predicted range in the emission rate, resulting from nonconstant speeds combined with a larger HDV percentage, in the morning (Fig. 4c) is large enough to explain the mismatch observed during the morning rush hour.

4 Discussion

The strategic reduction of emissions from transportation is important for both reducing total GHG emissions and improving AQ. To make informed decisions that reduce GHGs and exposure to poor AQ, policy makers need to know (1) how much is being emitted, (2) the location and timing of emissions, and (3) the relative impact of various subsector processes (e.g., vehicle kilometers and fleet composition).

To effectively capture emissions from subsector processes, models are also reliant on emission factor models, such as the EMFAC2017 model used in this paper. While our BEACO$_2$N-STILT-based estimates largely agree with EM-

FAC2017 with respect to CO_2, tracking on-road changes in emission factors will be especially important as the impacts of congestion and fleet composition evolve rapidly, making timely updates essential to creating spatially accurate inventories. For example, the EMFAC model predicts an 18 % decrease in overall CO_2 emission rates by 2030, resulting from the improved fuel efficiency of combustion engine vehicles and a transition to hybrid vehicles and EVs (~ 6.8 % of LDV vehicle kilometers and ~ 6 % of HDV vehicle kilometers are expected to be traveled by EVs by 2030). While the increased share of hybrid vehicles and EVs should work to decrease the impact of congestion, a projected increase in total congestion and the congested vehicle kilometer share by HDVs (Texas A&M Transportation Institute, 2019) is likely to work against that trend, making the overall result difficult to predict.

To our knowledge, this paper represents the first demonstration that a high-density atmospheric observing network can both diagnose and quantify the relative contributions of subsector processes at the neighborhood scale. We demonstrate that the BEACO$_2$N network (~ 2 km spacing) of low-cost CO_2 sensors can be used to quantify emission rates at a specific location (a ~ 5 km stretch) and by time of day. We show that, on the highway stretch examined, activity-based emission estimates that account for speed and HDV percentage match the inference from atmospheric measurements to within 3 %. Finally, we demonstrate that the BEACO$_2$N-STILT system detects daily changes in fuel efficiency that range from 200 to 300 g CO_2 per vehicle kilometer and that this system would be capable of detecting fleet-wide changes in fuel efficiency in ~ 3 years.

5 Outlook

In this work, we have demonstrated that the BEACO$_2$N-STILT system was able to infer emission rates from vehicles along a specific stretch of highway. To understand the extent to which this method can be applied to other contexts, future work should investigate the extent to which various elements of the BEACO$_2$N-STILT system, including measurement density, error in meteorology used to calculate STILT trajectories, and the quality of the prior, impact the ability of similar systems to estimate emissions.

For example, it is possible that the mismatch that we observe during the morning rush hour may be due to a larger relative meteorological model error in the morning compared with the afternoon and early evening, during which time the boundary layer is relatively well mixed. Because a highly mixed boundary layer is important for minimizing discrepancies between particle trajectories in the STILT model and real transport (Lin et al., 2003), inversions typically use only measurements taken during the afternoon, (Lauvaux et al., 2016, 2020; Nathan et al., 2019) when the boundary layer is relatively well mixed. However, as discussed by Martin et

al. (2019), the impacts of meteorological mismatch during the morning may be offset by a stronger signal, and future work should explore the extent to which averaging results over long time periods or strategic filtering of meteorological mismatches can combat emission error.

Beyond further exploration of the elements influencing the sensitivity and precision of the BEACO$_2$N-STILT system, because each BEACO$_2$N node measures CO, NO$_x$, and PM$_{2.5}$ in addition to CO_2 (Kim et al., 2018), the method presented in this paper has the potential to shed light on subsector processes impacting the emission factors of these co-emitted species. This is salient because plume-based emission factor measurements of co-emitted pollutants show that various emission factor models systematically underestimate emissions (Bishop, 2021), fail to capture spatial heterogeneity in these factors due to fleet composition (age and compliance with control technologies) for PM (Haugen et al., 2018; Park, et al., 2016) and black carbon (Preble et al., 2018), or fail to capture the impact of temperature on emission factors.

Applying these methods across a broader spatial area and to other species (e.g., PM$_{2.5}$, NO$_x$, and CO) should yield information of interest to both scientists and policy makers by

1. revealing spatial and temporal trends in emission rates and emission factors across an urban area and quantifying the contributions of congestion, fleet composition, or other factors to spatial variations;

2. identifying and diagnosing the causes of traffic-related AQ hot spots that contribute to exposure inequities;

3. tracking trends in the above over periods of years to decades.

Author contributions. HLF derived the CO_2 emissions from traffic data, conceived the idea for the project design, wrote the paper, and collected CO_2 data. AJT created and ran the CO_2 inversion code. HLF, JK, KC, ERD, CN, and PW collected CO_2 data. RCC gave feedback on the project design and assisted with writing the paper.

References

Apte, J. S., Messier, K. P., Gani, S., Brauer, M., Kirchstetter, T. W., Lunden, M. M., Marshall, J. D., Portier, C. J., Vermeulen, R. C. H., and Hamburg, S. P.: High-Resolution Air Pollution Mapping with Google Street View Cars: Exploiting Big Data, Environ. Sci. Technol., 51, 6999–7008. https://doi.org/10.1021/acs.est.7b00891, 2017.

Bay Area Air Quality Management District – BAAQMD: Bay Area Emissions Inventory Summary Report Base Year 2011, https://www.baaqmd.gov/~/media/files/planning-and-research/emission-inventory/by2011_ghgsummary.pdf (last access: 15 March 2022), 2015.

Bishop, G. A.: Does California's EMFAC2017 vehicle emissions model underpredict California light-duty gasoline vehicle NO_x emissions?, J. Air Waste Ma., 71, 597–606, https://doi.org/10.1080/10962247.2020.1869121, 2021.

Boswell, M. R. and Madilyn Jacobson, A. R.: 2019 Report on the State of Climate Action Plans in California, https://ww2.arb.ca.gov/sites/default/files/2020-03/17RD033.pdf (last access: 12 January 2022), 2019.

California Air Resources Board: PROGRESS REPORT: California's Sustainable Communities and Climate Protection Act, (November), 96, https://ww2.arb.ca.gov/sites/default/files/2018-11/Final2018Report_SB150_112618_02_Report.pdf (last access: 12 January 2022), 2018.

California Department of Transportation: Performance Measurement System, California Department of Transportation [data set], https://pems.dot.ca.gov, last access: 15 March 2022.

Caubel, J. J., Cados, T. E., Preble, C. V., and Kirchstetter, T. W.: A Distributed Network of 100 Black Carbon Sensors for 100 Days of Air Quality Monitoring in West Oakland, California, Environ. Sci. Technol., 53, 7564–7573, https://doi.org/10.1021/acs.est.9b00282, 2019.

Cohen Research – University of California Berkeley: Berkeley Environmental Air-quality & CO_2 Network (BEACO2N), http://beacon.berkeley.edu, last access: 15 March 2022.

Davis, S. C., Diegel, S. W., and Boundy, R. G.: Transportation Energy Data Book, Edition 29, Energy, https://tedb.ornl.gov/wp-content/uploads/2021/02/TEDB_Ed_39.pdf (last access: 12 January 2022), 2021.

City of Oakland: Oakland Equitable Climate Action Plan, https://cao-94612.s3.amazonaws.com/documents/Oakland-ECAP-07-24.pdf (last access: 12 January 2022), 2020

Delaria, E. R., Kim, J., Fitzmaurice, H. L., Newman, C., Wooldridge, P. J., Worthington, K., and Cohen, R. C.: The Berkeley Environmental Air-quality and CO_2 Network: field calibrations of sensor temperature dependence and assessment of network scale CO_2 accuracy, Atmos. Meas. Tech., 14, 5487–5500, https://doi.org/10.5194/amt-14-5487-2021, 2021.

Gately, C. K. and Hutyra, L. R.: Large Uncertainties in Urban-Scale Carbon Emissions, J. Geophys. Res.-Atmos., 122, 11242–11260, https://doi.org/10.1002/2017JD027359, 2017.

Gately, C. K., Hutyra, L. R., and Wing, I. S.: Cities, traffic, and CO_2: A multidecadal assessment of trends, drivers, and scaling relationships. P. Natl. Acad. Sci. USA, 112, 4999–5004, https://doi.org/10.1073/pnas.1421723112, 2015.

Gately, C. K., Hutyra, L. R., Peterson, S., and Sue Wing, I.: Urban emissions hotspots: Quantifying vehicle congestion and air pollution using mobile phone GPS data, Environ. Pollut., 229, 496–504, https://doi.org/10.1016/j.envpol.2017.05.091, 2017.

Gurney, K. R., Razlivanov, I., Song, Y., Zhou, Y., Benes, B., and Abdul-Massih, M.: Quantification of fossil fuel CO_2 emissions on the building/street scale for a large U.S. City, Environ. Sci. Technol., 46, 12194–12202, https://doi.org/10.1021/es3011282, 2012.

Gurney, K. R., Liang, J., Roest, G., Song, Y., Mueller, K., and Lauvaux, T.: Under-reporting of greenhouse gas emissions in U.S. cities, Nat. Commun., 12, 1–7, https://doi.org/10.1038/s41467-020-20871-0, 2021.

Haugen, M. J. and Bishop, G. A.: Long-Term Fuel-Specific NO_x and Particle Emission Trends for In-Use Heavy-Duty Vehicles in California, Environ. Sci. Technol., 52, 6070–6076, https://doi.org/10.1021/acs.est.8b00621, 2018.

Kim, J., Shusterman, A. A., Lieschke, K. J., Newman, C., and Cohen, R. C.: The BErkeley Atmospheric CO_2 Observation Network: field calibration and evaluation of low-cost air quality sensors, Atmos. Meas. Tech., 11, 1937–1946, https://doi.org/10.5194/amt-11-1937-2018, 2018.

Kim, J. Turner, A. J., Fitzmaurice, H. L., Delaria, E. R., Newman, C., Wooldridge, P. J., and Cohen, R. C.: Observing annual trends in vehicular CO_2 emissions, Environ. Sci. Technol., in review, 2021.

Kwon, J., Varaiya, P., and Skabardonis, A. Estimation of Truck Traffic Volume from Single Loop Detectors with Lane-to-Lane Speed Correlation, Transp. Res. Rec., 684, 106–117, https://doi.org/10.3141/1856-11, 2003.

Lauvaux, T., Miles, N. L., Deng, A., Richardson, S. J., Cambaliza, M. O., Davis, K. J., Gaudet, B. Gurney, K. R., Huang, J. O'Keefe, D., Song, Y., Karion, A., Oda, T., Patarsuk, R., Razlivanov, I., Sarmiento, D., Shepson, P, Sweeney, C. Turnbull, J., and Wu, K.: High-resolution atmospheric inversion of urban

CO_2 emissions during the dormant season of the Indianapolis flux experiment (INFLUX), J. Geophys. Res., 121, 5213–5236, https://doi.org/10.1002/2015JD024473, 2016.

Lauvaux, T., Gurney, K. R., Miles, N. L., Davis, K. J., Richardson, S. J., Deng, A., Nathan, B. J., Oda, T. Wang, J. A., Hutyra, L., and Turnbull, J.: Policy-relevant assessment of urban CO_2 emissions, Environ. Sci. Technol., 54, 10237–10245, https://doi.org/10.1021/acs.est.0c00343, 2020.

Lin, J. C., Gerbig, C., Wofsy, S. C., Andrews, A. E., Daube, B. C., Davis, K. J., and Grainger, C. A.: A near-field tool for simulating the upstream influence of atmospheric observations: The Stochastic Time-Inverted Lagrangian Transport (STILT) model, J. Geophys. Res.-Atmos., 108, 4493, https://doi.org/10.1029/2002JD003161, 2003.

Martin, C. R., Zeng, N., Karion, A., Mueller, K., Ghosh, S., Lopez-Coto, I., Gurney, K. R., Oda, T., Prasad, K., Liu, Y., and Dickerson, R.R., Investigating sources of variability and error in simulations of carbon dioxide in an urban region, Atmos. Environ., 199, 55–69, https://doi.org/10.1016/j.atmosenv.2018.11.013, 2019.

McDonald, B. C., McBride, Z. C., Martin, E. W., and Harley, R. A.: High-resolution mapping of motor vehicle carbon dioxide emissions, J. Geophys. Res.-Atmos., 119, 5283–5298, https://doi.org/10.1002/2013JD021219, 2014.

Moua, F.: California Annual Fuel Outlet Report Results (CEC-A15), Energy Assessments Division, California Energy Comission, https://www.energy.ca.gov/media/3874 (last access: 13 January 2022), 2020.

Nathan, B. J., Lauvaux, T., Turnbull, J. C., Richardson, S. J., Miles, N. L. and Gurney, K. R., Source sector attribution of CO_2 emissions using an urban CO/CO_2 Bayesian inversion system, J. Geophys. Res.-Atmos., 123, 13–611, https://doi.org/10.1029/2018JD029231, 2018.

Newman, S., Xu, X., Gurney, K. R., Hsu, Y. K., Li, K. F., Jiang, X., Keeling, R., Feng, S., O'Keefe, D., Patarasuk, R., Wong, K. W., Rao, P., Fischer, M. L., and Yung, Y. L.: Toward consistency between trends in bottom-up CO_2 emissions and top-down atmospheric measurements in the Los Angeles megacity, Atmos. Chem. Phys., 16, 3843–3863, https://doi.org/10.5194/acp-16-3843-2016, 2016.

Park, S. S., Vijayan, A., Mara, S. L., and Herner, J. D.: Investigating the real-world emission characteristics of light-duty gasoline vehicles and their relationship to local socioeconomic conditions in three communities in Los Angeles, California, J. Air Waste Ma., 66, 1031–1044, https://doi.org/10.1080/10962247.2016.1197166, 2016.

Preble, C. V., Cados, T. E., Harley, R. A., and Kirchstetter, T. W.: In-Use Performance and Durability of Particle Filters on Heavy-Duty Diesel Trucks, Environ. Sci. Technol., 52, 11913–11921, https://doi.org/10.1021/acs.est.8b02977, 2018.

Seto K. C., Dhakal, S., Bigio, A., Blanco, H., Delgado, G. C., Dewar, D., Huang, L., Inaba, A., Kansal, A., Lwasa, S., McMahon, J. E., Müller, D. B., Murakami, J., Nagendra, H., and Ramaswami, A.: Human Settlements, Infrastructure and Spatial Planning. In: Climate Change 2014: Mitigation of Climate Change. Contribution of Working Group III to the Fifth Assessment Report of the Intergovernmental Panel on Climate Change, edited by: Edenhofer, O., Pichs-Madruga, R., Sokona, Y., Farahani, E., Kadner, S., Seyboth, K., Adler, A., Baum, I., Brunner, S., Eickemeier, P., Kriemann, B., Savolainen, J., Schlömer, S., von Stechow, C., Zwickel, T., and Minx, J. C., Cambridge University Press, Cambridge, United Kingdom and New York, NY, USA, https://www.ipcc.ch/site/assets/uploads/2018/02/ipcc_wg3_ar5_chapter12.pdf (last access: 18 March 2022), 2014.

Shusterman, A. A., Teige, V. E., Turner, A. J., Newman, C., Kim, J., and Cohen, R. C.: The BErkeley Atmospheric CO_2 Observation Network: initial evaluation, Atmos. Chem. Phys., 16, 13449–13463, https://doi.org/10.5194/acp-16-13449-2016, 2016.

Tessum, C. W., Paolella, D. A., Chambliss, S. E., Apte, J. S., Hill, J. D., and Marshall, J. D.: $PM_{2.5}$ polluters disproportionately and systemically affect people of color in the United States, Science Advances, 7, 1–7, https://doi.org/10.1126/sciadv.abf4491, 2021.

Texas A&M Transportation Institute: Urban Mobility Report 2019, 182, https://static.tti.tamu.edu/tti.tamu.edu/documents/umr/archive/mobility-report-2019.pdf (last access: 13 January 2022), 2019.

Turner, A. J., Shusterman, A. A., McDonald, B. C., Teige, V., Harley, R. A., and Cohen, R. C.: Network design for quantifying urban CO_2 emissions: assessing trade-offs between precision and network density, Atmos. Chem. Phys., 16, 13465–13475, https://doi.org/10.5194/acp-16-13465-2016, 2016.

Turner, A. J., Kim, J., Fitzmaurice, H., Newman, C., Worthington, K., Chan, K., Wooldridge, P. J., Köehler, P., Frankenberg, C., and Cohen, R. C.: Observed impacts of COVID-19 on urban CO_2 Emissions, Geophys. Res. Lett., 47, p.e2020GL090037, Geophys. Res. Lett., 47, 1–6, https://doi.org/10.1029/2020GL090037, 2020a.

Turner, A. J., Köhler, P., Magney, T. S., Frankenberg, C., Fung, I., and Cohen, R. C.: A double peak in the seasonality of California's photosynthesis as observed from space, Biogeosciences, 17, 405–422, https://doi.org/10.5194/bg-17-405-2020, 2020b.